Published as: Mphateng, T.N., Mapossa, A.B., Wesley-Smith, J., Ramjee, S. and Focke, W.W., 2022. Cellulose acetate/organoclay nanocomposites as controlled release matrices for pest control applications. *Cellulose*, *29*(7), pp.3915-3933.

Cellulose Acetate/Organoclay Nanocomposites as Controlled Release Matrices for Pest Control Applications

Thabang N. Mphateng [a], António B. Mapossa [a,b*], James Wesley-Smith [c], Shatish Ramjee [a], Walter W. Focke [a,b]

[a]*Institute of Applied Materials, Department of Chemical Engineering, University of Pretoria, Private Bag X20, Hatfield 0028, Pretoria, South Africa*

[b]*UP Institute for Sustainable Malaria Control & MRC Collaborating Centre for Malaria Research, University of Pretoria, Private Bag X20, Hatfield 0028, Pretoria, South Africa*

[c]*Electron Microscope Unit, Sefako Makgatho Health Sciences University, Ga-Rankuwa 0208, South Africa*

[*]Corresponding author: mapossabenjox@gmail.com

Abstract

This study aimed to develop cellulose-based polymer matrices as controlled release devices for plant-based insect repellents and attractants, with the aim of finding sustainable and environmentally friendly pest control methods for agricultural applications. Citronellol, terpineol and methyl salicylate were the selected active compounds for this study. Their compatibility with cellulose diacetate was predicted using Hansen Solubility Parameters, which predicted terpineol as the most compatible with cellulose diacetate, followed by methyl salicylate and citronellol. This was consistent with the plasticization efficiency trend from DMA results of solvent cast cellulose diacetate films containing the active compounds. The chemical identity of the films and cellulose diacetate-active compound intermolecular interactions were verified by FTIR. TGA demonstrated the thermal stability of cellulose diacetate/active compound/clay formulations at temperatures not exceeding 170 °C. Cellulose diacetate/organoclay nanocomposite matrices containing the active compounds at 35 wt-% were prepared by twin screw extrusion compounding, with the active compounds also functioning as plasticizers. The amount of active compound in the strands was determined by solvent extraction and TGA. Both methods showed that small amounts of active compound were lost during the compounding process. SEM demonstrated the effect of organoclay on the internal morphology of the matrix, whereas TEM showed clay dispersion and intercalation within the matrix. The matrix served as a reservoir for the active compounds while simultaneously controlling their release into the environment. Release profiles, obtained through oven ageing at 40 °C for 70 days, were fitted to existing Log-logistic and Weibull models, and novel Diffusion and Modified Weibull release models. Citronellol was released the fastest, followed by methyl salicylate and terpineol. The findings suggest that cellulose diacetate/organoclay strands are promising controlled-release matrices for pest control purposes.

Keywords: Cellulose diacetate; controlled release; organoclay; nanocomposite; plasticizer efficiency; pest control.

Introduction

The agricultural sector represents a major sector of the economy of most countries. Fruit, vegetables, and small grain cereals have become invaluable for agricultural development in sub-Saharan African countries due to their nutritional value and economic returns (Martin et al., 2018, Botha et al., 2017). Fresh crop production depends on factors such as climatic conditions, availability of water for irrigation and soil fertility. Unfortunately, the agricultural sector is plagued by persisting problems caused by insect pests. They directly damage crops by feeding on them, but more importantly, indirectly by transmitting viral pathogens (Guerrieri and Digilio, 2008, Martin et al., 2018). Therefore, synthetic pesticides are applied to protect crops against insect pests. While they are effective in killing insects, synthetic pesticides have come under major scrutiny in recent times due to health, environmental, economic and ecological concerns (Koul et al., 2008). Recent studies have noted a dramatic plunge in insect numbers, the primary pollinators important for the maintenance of plant diversity, crop production and food security (Potts et al., 2010). This is most likely due to the uncontrolled and widespread use of pesticides (Ewald et al., 2015). The indiscriminate and excessive use of chemical pesticides leads to resistance, resurgence, persistent residues. It upsets the ecological balance by killing all insects, not only those that pose problems, but also the natural enemies.

Push-pull insect control, which involves behavioural manipulation of insect pests, may offer a more environmentally acceptable approach (Miller and Cowles, 1990, Said-Al Ahl et al., 2017). This biological control strategy integrates stimuli that make the protected crops unattractive to the pests (push) while luring them toward an attractive source (pull) from where the pests are subsequently eliminated (Cook et al., 2007). Push-pull approaches could exploit semiochemicals, i.e. compounds that convey a signal from one organism to another so as to modify the behaviour of the recipient organism (Law and Regnier, 1971). The plant-based active compounds considered in this study are citronellol, terpineol and methyl salicylate. Citronellol is an attractant for mites and western flower thrips (*Frankliniella occidentalis*) (Koschier et al., 2000), and a repellent for the sweet potato whitefly (*Bemisia tabaci*) (Baldin et al., 2014, Deletre et al., 2016, A Saad et al., 2017). α-Terpineol is a repellent for green peach aphids (*Myzus persicae*) (Dardouri et al., 2019), two-spotted spider mites (*Tetranychus urticae)* (da Camara et al., 2015, Tak and Isman, 2017) and tobacco beetles (*Lasioderma serricorne)* (You et al., 2015). Methyl salicylate is a repellent for western flower thrips (Koschier, 2008, Picard et al., 2012, Chermenskaya et al., 2001) and black bean aphids (*Aphis fabae*) (Hardie et al., 1994). These are volatile compounds which degrade in the open environment. Effective pest management, that utilises such volatile compounds, depends on novel delivery approaches that will allow controlled release, at effective levels, over extended periods (Allsopp, 2014). Therefore, this study explored the possibility of trapping such active compounds in a cellulose-based biopolymer matrix.

Cellulose is an abundant natural polymer obtained from trees, with the *Eucalyptus* species being a major source (Puls et al., 2010, Leite et al., 2016). It is a homopolymer of glucose, with the monomers connected by β-1,4 linkages. In plants, cellulose is arranged in microfibrils which make up the cell walls. Due to the strong intramolecular- and intermolecular hydrogen bonding, which also results in a high crystallinity, cellulose features considerable stability and excellent mechanical properties (Brigham, 2018). However, the melting point of cellulose exceeds its thermal decomposition temperature, and it is therefore impossible for it to be processed by melt extrusion (Teramoto, 2015, Okhovat et al., 2015). Derivatisation of cellulose by esterification yields

thermoplastic polymers such as cellulose diacetate, cellulose acetate butyrate and cellulose acetate propionate. These polymers feature modified thermal properties that allow thermal processing by melt extrusion (Teramoto, 2015).

This study utilised cellulose diacetate, the properties and applications of which depend significantly on the degree of substitution (DS). The DS is the average number of substituent acetyl groups per anhydroglucose (β-glucopyranose) unit (Fei et al., 2017, Bao, 2015). Cellulose acetate polymers with a DS between 2.0 to 2.7 (dubbed cellulose diacetate) are semi-crystalline biodegradable thermoplastics. Grades with a DS exceeding 2.9 (cellulose triacetate) feature a higher crystallinity, are also easier to melt process, but are less biodegradable (Puls et al., 2010, Zepnik et al., 2013b). In contrast to cellulose, cellulose diacetate is soluble in common organic solvents and much less crystalline (Fei et al., 2017).

Cellulose diacetate is a stiff and brittle material. External plasticization of partially substituted cellulose acetate is necessary in order to turn it into a useful thermoplastic material (Zepnik et al., 2013a). The addition of low molecular weight plasticisers significantly reduces the glass transition temperature (T_g) improving material flexibility and toughness (Dreux et al., 2019). In addition, it reduces the melt viscosity thereby extending the thermal processing window to lower temperatures (Phuong et al., 2014, Leite et al., 2016, Zepnik et al., 2013b, Zepnik et al., 2013a).

In this study, the potential of cellulose diacetate strands as controlled release devices was investigated. The biodegradable cellulose-based matrix is to act as a reservoir for the desired active while simultaneously controlling its release into the environment. The active compounds were incorporated into the polymer matrix by an extrusion-compounding process which resulted in continuous plastic strands. These can be used as such or turned into nets that can serve as active plant protection devices to be installed in orchards and vegetable gardens. They can be used to either repel insect pests from important crops in pre- and post-harvest applications or as part of traps designed to capture and eliminate harmful insects. Alternatively, they can be used to attract beneficial insects such as natural predators of the troubling insect pests.

Materials and Methods

Materials

Cellulose diacetate (CA) powder (CAS No: 9035-69-2; DS = 2.4, Mn = 64787 Da, 54.7 % combined acetic acid content) was supplied by Haihang Industry (China). Sigma-Aldrich supplied terpineol (CAS No. 8000-41-7), methyl salicylate (CAS No. 119-36-8), citronellol (CAS No. 16-22-92) (95 % purity), triethyl citrate (CAS No. 77-93-0), methanol (CAS No. 67-56-1) (99.8 % purity) and dichloromethane (CAS No. 75-09-2) (99.8 % purity). Laviosa Chimica Mineraria SpA supplied the Dellite 43B organoclay. The organo-modifier was dimethyl benzyl hydrogenated tallow ammonium, and the mean particle size was 8 µm. All materials were used as received.

Cellulose diacetate was dried in a convection oven set at 80 °C for 24 h before it was used in the extrusion-compounding and solvent casting processes.

Volatility and air permeability

The air permeability of a compound determines the rate at which it migrates away from an exposed surface. It is defined as the product of the vapour pressure and the diffusion coefficient in air, as shown by Equation 1.

$$S_A = P_A^{sat} D_A \quad (1)$$

where S_A is the air permeability ($Pa \cdot m^2 s^{-1}$), P_A is the sample vapour pressure (Pa) at the measurement temperature T (K), and D_A is the diffusion coefficient of the compound in air ($m^2 \cdot s^{-1}$).

A gravimetric method, described by Mapossa et al. (2020) and Pieterse and Focke (2003) was used to compare the relative volatility of the repellents. Pre-weighed Payne permeability pans, containing ca. 18 g of a compound, were placed in a convection oven set at 40 °C. The mass loss of the repellents was tracked by weighing the pans daily over a period of one week. The evaporation rate ($\dot{m}$, $kg \cdot m^{-2} s^{-1}$) was calculated from the slope of the mass loss curve at the point where half the liquid had evaporated. S_A was determined from Equation 2:

$$S_A = zRT\dot{m}/M_A \quad (2)$$

where z (m) is the depth of the liquid in the pan at the point when half of it was lost; R (8.314 $J \cdot mol^{-1} K^{-1}$) is the gas constant, T is the absolute temperature in K, and M_A ($kg \cdot mol^{-1}$) is the molar mass of the compound. The experimental values determined for methyl salicylate were checked using the vapour pressure and diffusion coefficient reported at 40 °C by Kosina et al. (2013)

Equation 1 allows estimation of the diffusion coefficient in air if the vapour pressure is known. Unfortunately, available vapour pressure data or vapour pressure correlations for the present compounds did not extend to 40 °C. It was found necessary to extrapolate available data to the latter temperature using data regression based on the Antoine vapour pressure equation

($\ln P = A - B/(C + T)$), where P is the vapour pressure at temperature T, and B and C are Antoine constants.

Solvent casting

Cellulose diacetate/active compound mixtures were dissolved in a 50 ml binary solvent mixture consisting of 80 vol-% dichloromethane and 20 vol-% acetone. The solution was stirred at 500 rpm for 50 minutes at room temperature and then transferred to a glass Petri dish. It was partially covered with a second Petri dish to reduce the rate of solvent evaporation. The solvent was allowed to evaporate slowly, and the films were left to dry for at least 24 h at room temperature. It should be noted that 43B organoclay was added at 5 wt-% to the triethyl citrate and methyl salicylate formulations to facilitate the mixing process and improve film quality and dimensional stability.

Extrusion compounding

A typical formulation was prepared as follows: Cellulose diacetate powder (1200 g), citronellol (700 g) and Dellite 43B clay powder (100 g) were mixed in a 5-litre plastic container and the semi-dry blend was compounded in a Prism TSE 24 twin-screw co-rotating compounder (24 mm ϕ, 30 L/D) fitted with a 5.5 mm diameter die. The temperature profile, from feed to the die, was set at 80/120/150/150/170/170/170 °C and the screw speed was 125 rpm. The exiting molten strands were quenched by passing them through an ice-water bath. The diameters of the strands were measured with a Mitutoyo digital caliper.

Solvent extraction

Extruded strands containing the active compounds were cut to lengths of 50 ± 10 mm and weighed. Thereafter, they were placed in Polytop glass vials to which methanol was added before stoppering. The solvent was replaced on a daily basis. After completing the fifth extraction, the strands were removed and allowed to dry, first at ambient conditions, and then in a convection oven set to 40 °C. The mass of the methanol-free strands was determined, and the amount extracted was calculated. The average of triplicate evaluations is reported.

Dynamic mechanical analysis (DMA)

Dynamic mechanical analysis on a Perkin-Elmer DMA 8000 instrument was used to determine the glass transition temperature as a function of repellent content. Samples of the solvent-cast films, 30 mm long and 7 mm wide, were placed in Perkin-Elmer stainless steel material pockets. They were analysed in the single cantilever bending mode at a fixed frequency of 1 Hz. The samples were heated from 30 °C to 200 °C at a scan rate of 2 $K \cdot min^{-1}$.
The change in glass transition temperature was used to investigate the efficiency of the active compounds as plasticisers for cellulose diacetate. This was determined by the peak in the tan δ (E”/E’) curves (de Paula et al., 2019).
Stainless-steel pockets affect the loss (E”) and storage (E’) moduli results as the measured values represent the composite moduli of the pocket together with the films instead of the moduli of film on its own (Bier et al., 2012, de Paula et al., 2019). For this reason, the values of the moduli are not representative of the film and were neglected. However, the shape of the tan δ curve is still representative of the film and the peak, hence T_g, can be obtained.

Thermogravimetric analysis (TGA)

Thermal analysis was performed on a TA Instrument SDT-Q600 Simultaneous TGA/DSC. Samples, weighing 12 ± 2 mg were placed in 70 μL alumina cups. They were heated from ambient to 500 °C at 10 $K \cdot min^{-1}$ of heat flow. The purge gas was nitrogen flowing at a rate of 50 $mL \cdot min^{-1}$.

Fourier Transform Infrared (FTIR) spectroscopy

A Perkin-Elmer 100 spectrometer, fitted with a universal attenuated total reflectance (ATR) accessory, was used to determine the infrared spectra of the films and active compounds. The spectra were recorded in the absorbance region of 4000-400 cm^{-1} with a resolution of 4 cm^{-1} and an average of 16 scans.

Scanning electron microscopy (SEM)

Active compound-free polymer strands were immersed in liquid nitrogen for approximately 10 minutes and then fractured. The fracture surface was rendered conductive by coating with carbon using a Quorum Q150T ES sputter coater prior to analysis. The samples were viewed using a Zeiss Ultra 55 Field Emission Scanning Electron Microscope at an acceleration voltage of 3 kV and the magnification was varied between 20000 and 25000X.

Transmission electron microscopy (TEM)

Ultrathin sections of the strands, approximately 70 nm thickness, were prepared using a Leica UC7 ultramicrotome at room temperature. The organoclay dispersion in the cellulose diacetate matrix was examined in a JEOL JEM 1010 transmission electron microscope operated at an accelerating voltage of 100 kV.

Release profile of active compounds from cellulose diacetate strands by oven ageing

The release profiles of the repellents from the polymer strands were determined gravimetrically. Loose coils of the extruded strands were suspended in an EcoTherm-Labcon forced convection oven with the temperature set at 40 °C for 70 days. The coils were weighed on alternate days during the first two weeks and thereafter on a weekly basis.

Modelling of the release profiles of active compounds

Consider the release of an active compound that is initially homogeneously dispersed in the polymer matrix. The present strand-based matrix, with a circular cross-section, approximates to an infinite cylinder of diameter d containing the mobile active compound. It is assumed the latter rapidly evaporates as soon as it reaches the surface of the polymer matrix. This implies a diffusion limited release rate, i.e. that the evaporation of the active from the surface into the environment is much faster than the rate at which it can be replenished by diffusion from inside the strand. In addition, it is assumed that cellulose diacetate strands retain their original shape during this process and that the diffusion coefficient is a constant, i.e. it is neither a function of concentration nor distance. The differential equation describing this situation is:

$$\frac{\partial C}{\partial t} = \frac{1}{r}\frac{\partial}{\partial r}\left(rD\frac{\partial C}{\partial t}\right) \tag{3a}$$

With initial condition: $t = 0;\ 0 < r < d/2: \quad C = C_0$ (3b)

and boundary condition: $t>0;\quad r=d/2:\ C=0$ (3c)

Solutions to Equation 3 are presented in Crank (1975). The present interest is in $M(t)$, the amount of the active released from the strand at time t. Analysis yields an exact solution, that for a cylinder of radius a, takes the form of an infinite series of exponential terms (Crank, 1975):

$$\frac{M(t)}{M_\infty}=1-\sum_{n=1}^{\infty}\frac{16}{d^2\alpha_n^2}\exp\left(-D\alpha_n^2 t\right) \tag{4}$$

where the α_n values are obtained from the roots of $J_o(d\alpha_n/2)$, the Bessel function of the first kind of order zero. For the present analysis, the most important one is the first root which equals $d\alpha_o/2 = 2.40483$.

This series solution is inconvenient for practical applications as it converges very slowly. However, since the terms are exponentials, the first one dominates at long times. This leads to the long-time asymptote given by:

$$\frac{M(t)}{M_\infty}\approx 1-0.691658\exp\left(-23.13283\frac{Dt}{d^2}\right) \tag{5a}$$

or, more conveniently

$$\frac{M(t)}{M_\infty}\approx 1-0.691658\exp\left(-\frac{t}{\tau_\infty}\right) \tag{5b}$$

where $\tau_\infty = 0.043229\,d^2/D$ (6)

It is clear from Equation 5 that the repellent release follows an exponential decay law after a sufficiently long release time.

Crank (1975) also lists another mathematical solution, in the form of a series expansion, which converges fast for short times:

$$\frac{M(t)}{M_\infty}=\frac{8}{\sqrt{\pi}}\sqrt{\frac{Dt}{d^2}}-\frac{4Dt}{d^2}-\frac{1}{3}\left(\frac{4Dt}{d^2}\right)^{3/2}\ldots \tag{7}$$

Only the first term is important for very short times:

$$\frac{M(t)}{M_\infty}\approx\sqrt{\frac{64Dt}{\pi d^2}}=\sqrt{\frac{t}{\tau_o}} \tag{8}$$

Where $\tau_o=\frac{\pi d^2}{64D}$ (9)

Therefore, at very short times, the repellent release should follow a square root time dependence with a characteristic diffusion time constant τ_o. According to Equation 9, the latter is inversely proportional to the diffusivity of the molecules inside the material constituting the strand, and directly proportional to the square of the strand diameter (Ignacio et al., 2017). The functional form of Equation 8 was initially proposed by Higuchi (1961) to describe the release of a drug from a thin ointment film. The Peppas group critically evaluated the

Higuchi equation (Siepmann and Peppas, 2011) and empirically extended it, among other approaches, by considering exponents that differ from the square root time dependence (Ritger and Peppas, 1987). It is often stated that Equation 8 can be treated as an empirical relationship that is useful up to the point where 60 % of the active has been released. However, with the correct diffusion coefficient applied, the validity of the asymptotic relationship breaks down much earlier.

Note that Equation 8 predicts completion of the release of the active compound at time $t = \tau_o$. In reality, the release approaches completion only asymptotically and therefore takes a much longer time to even just reach, say, 95 % completion. It is preferable to have a simple correlating function capable of representing the entire time-dependent release profile. The simplest such model, which retains the short-time behaviour indicated by Equation 8 is the log-logistic function with the exponent set to $\beta = 0.5$:

$$\frac{M(t)}{M_\infty} = \frac{\left(t/\tau_o\right)^\beta}{1+\left(t/\tau_o\right)^\beta} \tag{10}$$

Marabi et al. (2003), Kosmidis et al. (2003), Papadopoulou et al. (2006) and Ignacio et al. (2017) explored the application of the Weibull distribution function as an empirical expression describing the release profile.

$$\frac{M(t)}{M_\infty} = 1 - \exp\left[\left(-t/\tau\right)^\beta\right] \tag{11}$$

It was deemed a promising candidate due to its high correlating flexibility. Indeed, Monte Carlo simulations have shown that it provides very good fits to diffusion-limited controlled-release curves for cylinders with the exponent n taking on values between $0.69 \le n \le 0.75$ (Papadopoulou et al., 2006, Kosmidis et al., 2003). This compares with a value of $\beta = 0.72$ recommended by Marabi et al. (2003). However, this naive Weibull approach does not reduce to the correct release behaviours expected for either very short times or for very long times. For example, the short-time behaviour implies that one should set $\beta = 0.5$. However, this does not yield the correct long-time behaviour of exponential decay. To remedy this, Ignacio et al. (2017) proposed a two-parameter modification which they claimed to deliver the correct asymptotes. It certainly does so for the one defined by Equation 9, valid for short times:

$$\frac{M(t)}{M_\infty} = 1 - \exp\left[-\sqrt{t/\tau_o + \left(t/\tau_\infty\right)^2}\right] \tag{12}$$

Ignacio et al. (2017) validated this suggestion using Monte Carlo simulations (Ignacio et al., 2017). Note that, since the differential Equation 3 clearly indicates that $M(t)/M_\infty = f\left(Fo\right)$ with $Fo = Dt/d^2$, therefore the two characteristic time constants in Equation 12 are not independent. The link is found by combining Equations 6 and 9:

$$\tau_\infty = 0.880646\,\tau_o \tag{13}$$

However, the Ignacio et al. (2017) approach does not actually reproduce the long-time asymptote defined by Equation 5 as the pre-exponential constant is absent. Churchill and Usagi (1972) and Churchill (2001) developed an alternative procedure for constructing a single correlating equation for processes that feature two limiting forms

conforming to the behaviour at large- and at small values of the independent variable. Their proposal for the interpolating expression is to take a power mean over the two asymptotic expressions. If these are denoted by $X_{t\to 0}$ for short times and $X_{t\to\infty}$ for long times, the result is:

$$X(t)=\left[X_{t\to o}^{n}+X_{t\to\infty}^{n}\right]^{1/n} \tag{14}$$

Applied to the present situation, the following is obtained:

$$X^{n}=\left(t/\tau_{o}\right)^{\frac{n}{2}}+\left[1-0.692\exp\left(-t/\tau_{\infty}\right)\right]^{n} \tag{15}$$

where the first and second terms represent the short-time ($X_{t\to 0}$) and long-time ($X_{t\to\infty}$) asymptotic functions, respectively.

Subject to a judicious choice of the power index n, such an approximation usually provides an accurate representation of the full behaviour, particularly the behaviour in the transition region (Churchill, 2001). According to Churchill and Usagi (1972), the resulting expression is not sensitive to the choice of n and they recommend that the closest integral value be chosen for simplicity. Therefore, a value of $n = -4$ was selected on the basis of the theoretical plot of the release behaviour by Crank (1975). Note that Equation 12 also applies to the time constants τ_o and τ_∞ in this model.

Results and Discussion

Volatility and air permeability of active compounds

Table 1 presents the air permeability, vapour pressure and diffusion coefficient values of the active compounds at 40 °C. Experimental S_A values show that citronellol is the least- and methyl salicylate the most volatile of the three compounds. The vapour pressures did not follow the same ranking as terpineol, and methyl salicylate switched places with the result that the vapour pressure increased in the order citronellol < methyl salicylate < terpineol. This is due to the diffusion coefficient for terpineol being much lower than that of methyl salicylate. This significantly lowered the air permeability despite the higher vapour pressure. It is noteworthy that the diffusion coefficient of methyl salicylate in this study was greater than those reported by Kosina et al. (2013) by a factor of 10.

Table 1 Calculated vapour pressures and experimental estimates of the diffusion coefficient and air permeability for the active compounds at 40 °C.

Active compound	S_A **(mPa·m²s⁻¹)**	P_A **(Pa)**	D_A **(cm²s⁻¹)**
Citronellol	0.224 ± 0.005	21.0	0.105 ± 0.011
Terpineol	0.970 ± 0.022	57.6	0.166 ± 0.017
Methyl salicylate	2.420 ± 0.050	49.0	0.494 ± 0.024

Compatibility of active compounds with cellulose diacetate

Compatibility of cellulose diacetate with citronellol, terpineol and methyl salicylate was predicted by applying the Hansen's solubility parameter method. The component solubility parameters were obtained from literature sources and used to determine the total solubility parameters of the compounds from Equation 16 as follows:

$$\delta_T = \sqrt{\delta_D^2 + \delta_P^2 + \delta_H^2} \quad (16)$$

whereby Hildebrand's solubility parameter was split into three fundamental intermolecular interactions; dispersion (δ_H), polarity (δ_P) and hydrogen bonding (δ_H) interactions (Wypych, 2019, Louwerse et al., 2017). Using Hansen's method, an approximately spherical solubility area can be constructed in a three-dimensional co-ordinate system, with the axes defined by the individual solubility parameters. The radius of this solubility sphere is referred to as the interaction radius (R_0), which is used to predict solubility between the solvent and the polymer (Ghorani et al., 2013). R_0 gives the boundary that separates good solvents from poor solvents, whereby solvents which are contained within the sphere have good compatibility with the polymer, and those outside the sphere are poor solvents (Batista et al., 2015). This prediction can be made by Equation 17 as follows:

$$\sqrt{4\left(\delta_{Ds} - \delta_{Dp}\right)^2 + \left(\delta_{Ps} - \delta_{Pp}\right)^2 + \left(\delta_{Hs} - \delta_{Hp}\right)^2} \quad (17)$$

whereby is the distance of the solvent from the centre of the polymer solubility sphere, and δ_{Xs} and δ_{Xp} are the Hansen component parameters for the solvent and polymer, respectively. From this equation, good polymer-solvent compatibility is most likely if $R_a < R_0$, and poor polymer-solvent compatibility is then indicated by $R_a > R_0$ (Garcia et al., 2009, Swapnil et al., 2020).

Table 2 presents the solubility parameters of the active compounds, which indicate good compatibility with cellulose diacetate, as indicated by the R_a-values, which are significantly less than the cellulose diacetate R_o-value. Terpineol has the lowest R_a value, followed by methyl salicylate and citronellol. As a result, terpineol is expected to be the most compatible AC, and also more compatible than triethyl citrate and triacetin, which are two of the most common plasticizers for cellulose diacetate. Citronellol is expected to be the least compatible with the polymer.

Table 2 Hansen solubility parameters for CA and the selected plasticizers and ACs.

	δ_D (MPa$^{1/2}$)	δ_P (MPa$^{1/2}$)	δ_H (MPa$^{1/2}$)	δ_T (MPa$^{1/2}$)	R_o (MPa$^{1/2}$)	R_a (MPa$^{1/2}$)
Cellulose diacetate	14.9	7.1	11.1	19.89	12.40	-
Triethyl Citrate	16.5	4.9	12.0	20.98	-	3.99
Triacetin	16.5	4.5	9.1	19.37	-	4.58
Terpineol	13.9	8.0	10.2	19.01	-	2.37
Citronellol	16.1	4.8	10.8	19.97	-	3.34
Methyl salicylate	16.0	8.0	12.3	21.71	-	2.66

Thermogravimetric analysis (TGA)

Fig. 1 shows the vaporisation behaviour of the three compounds as determined by thermogravimetric analysis. All three compounds started to evaporate below 100 °C and mass loss was completed well below 200 °C. The DTG peak temperatures were 170 °C, 181 °C and 189 °C for terpineol, methyl salicylate and citronellol respectively. Therefore, the TGA results indicate that terpineol was the most volatile and citronellol the least volatile of the three compounds. Surprisingly, this volatility ranking differs from the one found for evaporation at the constant temperature of 40 °C. At that temperature, methyl salicylate was more volatile than terpineol, but the TGA results indicate that the opposite is true at elevated temperature. Table 1 shows that terpineol already featured a higher vapour pressure than methyl salicylate at 40 °C. The lower volatility observed at the low temperature was caused by the comparatively much lower diffusion coefficient. The latter increases proportional to the 1.75 power of the absolute temperature while the vapour pressure, in effect, increases exponentially with temperature. This explains the change in the volatility ranking at the higher temperature employed in the TGA experiment.

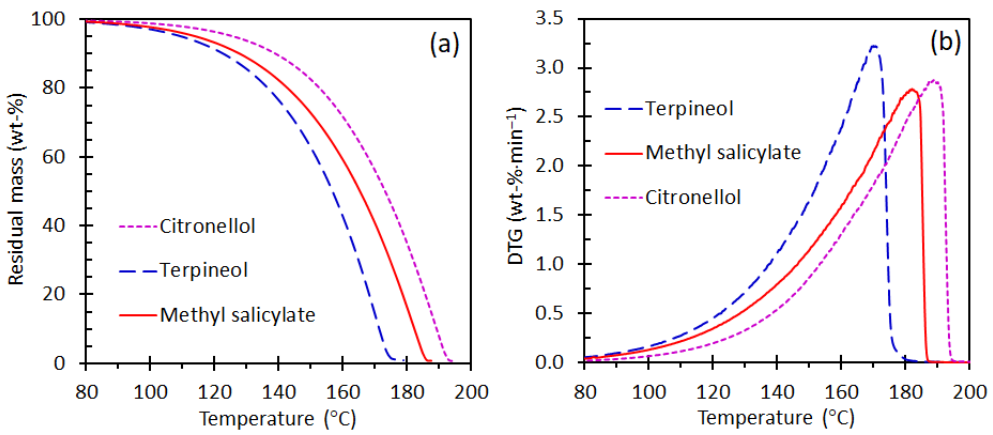

Fig. 1 Volatilisation behaviour of neat terpineol, methyl salicylate and citronellol shown by (a) TGA and (b) DTG curves

Fig. 2a shows mass loss curves for the neat cellulose diacetate, neat Dellite 43B organoclay and cellulose diacetate containing 7 wt-% of the clay. The first small mass loss steps, in the range 100 to 150 °C, are attributed to the evaporation of moisture present in the samples. It was about 1.3 wt-% for the clay and 5.2 wt-% for the cellulose diacetate. The loss of the intercalated organic surfactant, present in the clay, commenced at about 200 °C and it is due to a combination of volatilisation and decomposition. Most of this mass loss happens before about 300 °C but it continues gradually over a larger temperature range. The TGA mass loss at 450 °C suggests that the clay contained about 17 wt-% of the cationic surfactant. For the neat cellulose diacetate, the onset of thermal degradation is about 330 °C. Mass loss accelerated above that temperature with a mass loss of 50 wt-% recorded at 366 °C and becoming virtually complete at 400 °C. The mass loss curve for the cellulose diacetate compound containing 7 wt-% clay, suggests that the clay catalyses the degradation of the polymer. This is indicated by the observation that mass loss commences at an earlier temperature corresponding to the degradation onset temperature of the clay itself. This suggests that the volatilisation of the surfactant plays a role in the

decomposition of the material. However, the DTG curves (not provided) show that later, at a second stage, the clay itself also acts as an apparent degradation catalyst. The result is that the polymer/organoclay degradation commenced in earnest about 40 °C earlier compared to the neat polymer. These observations were considered when selecting the processing temperature employed during the extrusion compounding of the strands. Fortunately, it proved possible to perform the processing at temperatures that did not exceed 170 °C. At this temperature neither the clay nor the polymer is expected to suffer significant degradation considering the exposure to elevated temperatures was quite short, in the order of a few minutes.

Fig. 2b shows the TGA curves recorded for the extrusion-compounded samples containing 35 wt-% repellent and 5 wt-% clay. The DTG peak temperatures corresponding to the vaporisation of the repellents shifted to 216 °C, 238 °C and 225 °C for terpineol, methyl salicylate and citronellol respectively. This shows that the incorporation of the repellents in the cellulose diacetate matrix significantly delayed volatilisation. Interestingly, these DTG peak temperatures closely match the normal boiling points of the terpineol (T_b = 219 °C) and the citronellol (T_b = 225 °C). However, it is higher than the normal boiling point of methyl salicylate (T_b = 220 °C) implying that this repellent is more strongly held by the cellulose diacetate matrix.

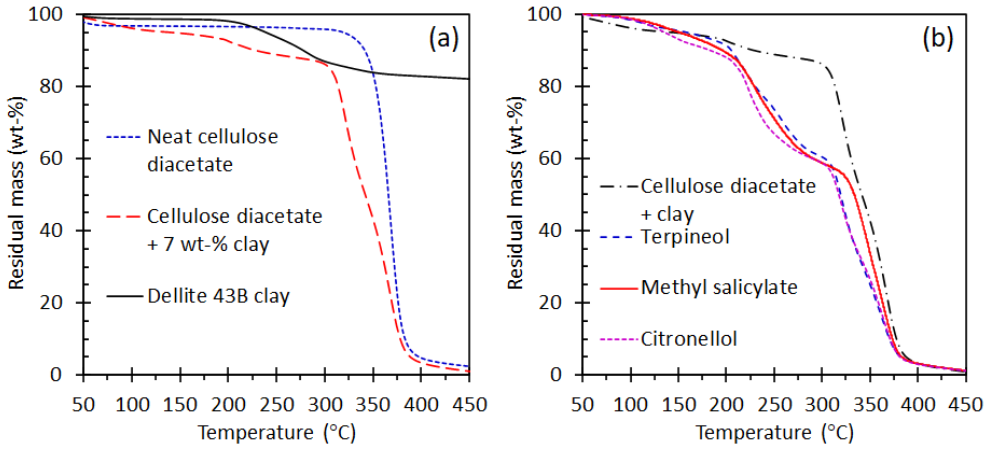

Fig. 2 (a) TGA curves for neat cellulose diacetate, cellulose diacetate containing 7 wt-% clay and neat organoclay Dellite 43B. (b) TGA curves of compounds containing nominally 35 wt-% repellent and 5 wt-% clay compared to that for the cellulose diacetate containing 7 wt-% clay

Fourier Transform Infrared (FTIR) spectroscopy

Fig. 3 shows the FTIR spectra of solvent cast cellulose diacetate films. Cellulose diacetate had characteristic bands at 1737 cm^{-1} (C=O stretching vibration in acetyl groups), 1368 cm^{-1} (C-H bending vibration of CH_3 in acetyl groups), 1220 cm^{-1} (C-O-C asymmetric stretching vibration in ester groups), 1035 cm^{-1} (C-O-C stretching vibration due to the glycosidic bond between the pyranose rings) and the broad hydroxyl group band in the 3700 and 3100 cm^{-1} region, peaking at 3466 cm^{-1} (Zhang et al., 2020, Jatoi et al., 2020, Fei et al., 2017, Gopi et al., 2019).

Characteristic IR absorption peaks for cellulose diacetate-citronellol (CA-CIT) films are shown in Fig. 3a. A distinct citronellol absorption peak appears in the film formulations between 3000 cm^{-1} and 2780 cm^{-1}, with the

highest absorption peak at 2914 cm^{-1} due to C-H stretching (Songkro et al., 2011), which also becomes more prominent as the concentration of citronellol in the films increased. Cellulose diacetate-terpineol (CA-TER) films also display a similar trend, with the C-H stretching at 3000 – 2800 cm^{-1} becoming more prominent as the terpineol amount was increased in the CA-TER film formulations. The IR spectra for the cellulose diacetate-methyl salicylate (CA-MET) films also displayed distinct methyl salicylate absorption peaks appear between 1680 and 700 cm^{-1}, with the ester C=O group at 1677 cm^{-1} and the aromatic C=C stretching vibrations between 1615 and 1439 cm^{-1} being the most notable (Kujur et al., 2019, Silva et al., 2020, Lee et al., 2020). The broad -OH bands are shown in Fig. 3b, which illustrate the increase in width and intensity in the citronellol and terpineol films, attributed to the increased hydrogen bonding interactions (Sudiarti et al., 2017, Teixeira et al., 2021). However, the methyl salicylate film showed a significant decrease in the area and peak intensity due to the sterically hindered -OH group of this compound, which weakened the hydrogen bonds. Fig. 3c compares the positions of the carbonyl peaks for CA-CIT, CA-TER and CA-MET films at 35 wt-% of the active compound, which illustrate the hydrogen bonding of -OH groups of the active compounds with the carbonyl groups of cellulose diacetate. The C=O peak of the citronellol film shifted to a higher wavenumber (1743 cm^{-1}), followed by methyl salicylate (1742 cm^{-1}) and terpineol (1741 cm^{-1}), which also implies that the carbonyl-hydroxyl hydrogen bonding between CA and the ACs was similar. Fig. 3d demonstrates the effects of hydrogen bonding on the absorption peaks of the carbonyl functional group in the CA-CIT films. The peaks shifted to higher wavenumbers as the citronellol concentration increased in the films, which confirms the intermolecular interaction between the polymer and citronellol, particularly hydrogen bonding. This also verifies the compatibility as predicted by the solubility parameters. Furthermore, the shifting of carbonyl absorption peaks to higher wavenumbers also signifies the weakening of the hydrogen bonding as the concentration of citronellol increased. This trend was also observed in the terpineol and methyl salicylate film formulations. Overall, Fig. 3 demonstrates a consistent chemical identity for the film formulations, which is a hybrid of the neat CA and the AC. This proves that the active compounds were indeed trapped into the cellulose diacetate films. The absence of new functional groups within the films is an indication that the polymer and the respective AC did not undergo any chemical modification during the preparation of the films.

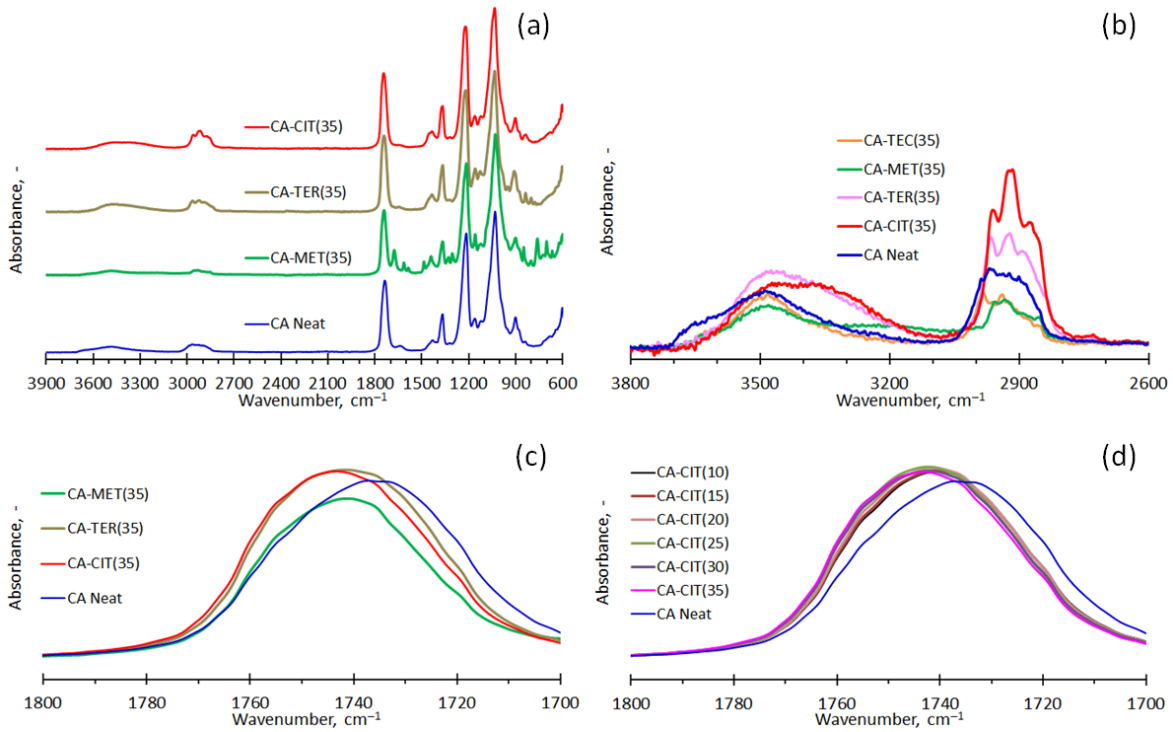

Fig. 3 FTIR spectra of solvent cast cellulose diacetate films. (a) Neat cellulose diacetate, and cellulose diacetate containing 35 wt-% citronellol, terpineol and methyl salicylate. (b) Carbonyl absorption peaks of neat cellulose diacetate, and cellulose diacetate containing 35 wt-% citronellol, terpineol and methyl salicylate. (c) Carbonyl absorption peaks of neat CA film and CA-citronellol films at 10 to 35 wt-% citronellol, at 5 wt-% increments

DMA and Plasticization efficiency

Cellulose diacetate is a brittle material. Plasticization improves the ductility and facilitates melt processing. It was therefore of interest to determine whether the present active compounds could provide the necessary plasticization effect. If that were the case, it would obviate the need to include a conventional plasticizer in the formulations. Mauritz et al. (1990) defined a plasticizer efficiency parameter, *k*, which is defined by a linear equation that shows the decrease in the polymer glass transition temperature in proportion to the amount of plasticizer added:

$$T_g = T_{g,2} - kw_1 \tag{16}$$

The constant *k* uniquely captures the plasticization efficiency of a candidate diluent in the low-to-moderate diluent concentration range. The variation of the glass transition temperature with diluent content is usually bracketed by the predictions defined by the linear blending rule as an upper bound;

$$T_g = T_{g1} w_1 + T_{g2}\left(1 - w_1\right) \tag{17}$$

and the Fox equation as a lower bound:

$$\frac{1}{T_g} = \frac{w_1}{T_{g,1}} + \frac{1-w_1}{T_{g,2}} \tag{18}$$

In these two equations, $T_{g,1}$ and $T_{g,2}$ are the glass transition temperatures of the diluent and the polymer respectively, and w_1 is the mass fraction of the diluent in the compound. This means that the plasticization efficiency parameter k in the Mauritz et al. (1990) expression, i.e. eq 16, is expected to vary between the following extreme values:

$$T_{g,2} - T_{g,1} \leq k \leq \frac{T_{g,2}}{T_{g,1}}\left(T_{g,2} - T_{g,1}\right) \tag{19}$$

The experimental T_g for the neat cellulose diacetate was 192.3 °C. This agrees with T_g values reported in the literature for cellulose diacetate grades with a DS of 2.4 to 2.5 (Bao et al., 2015, McBrierty et al., 1996, Ferfera-Harrar and Dairi, 2014, Quintana et al., 2013). DMA curves presented in Fig. 4a show that all formulations had only one distinct tan δ peak, positioned at a temperature that was significantly lower than the one for the neat cellulose diacetate. This verifies the compatibility of the active compounds with cellulose diacetate and demonstrates that they can be used as plasticizers.

Fig. 4b compares the DMA-determined glass transition temperatures determined from the position of the maxima in the tan δ peaks. The ratio of the measured values, relative to the value for the neat cellulose diacetate are plotted. This was done in order to allow comparisons to be made in terms of the plasticizer efficiency parameter proposed by Mauritz et al. (1990), i.e. Equation 16. To provide perspective, DMA-derived data for two actual plasticizers, i.e., triethyl citrate and triacetin, are included. The values for the triethyl citrate were measured presently. The values for triacetin, reported by Erdmann et al. (2021) and Bao (2015), are shown as filled circles together with the corresponding linear regression line as per Equation 18. The envelope curves for triacetin, defined by the linear blending rule (Equation 19) and the Fox equation (Equation 20) are also plotted. The normalized T_g point values for triethyl citrate and terpineol lie below the regression for triacetin. This suggests that both compounds are more efficient plasticizers for cellulose diacetate. The points for citronellol and methyl salicylate are initially also lower, but the glass transition temperature then approaches a plateau at an active content of 20 wt-% and beyond. Such a trend is consistent with a limited solubility of these actives in the cellulose diacetate matrix. Above the solubility limit, the system phase separates. The two phases feature different T_g values, and their observation would provide further proof that phase separation had indeed occurred. Unfortunately, it was not possible to scan lower temperatures with the DMA setup available to the present study. Nevertheless, Figure 4 provides evidence that citronellol, methyl salicylate and especially terpineol, are indeed excellent plasticizers for cellulose diacetate. Therefore, it was deemed not necessary to include a conventional plasticizer in the extruded polymer strand formulations.

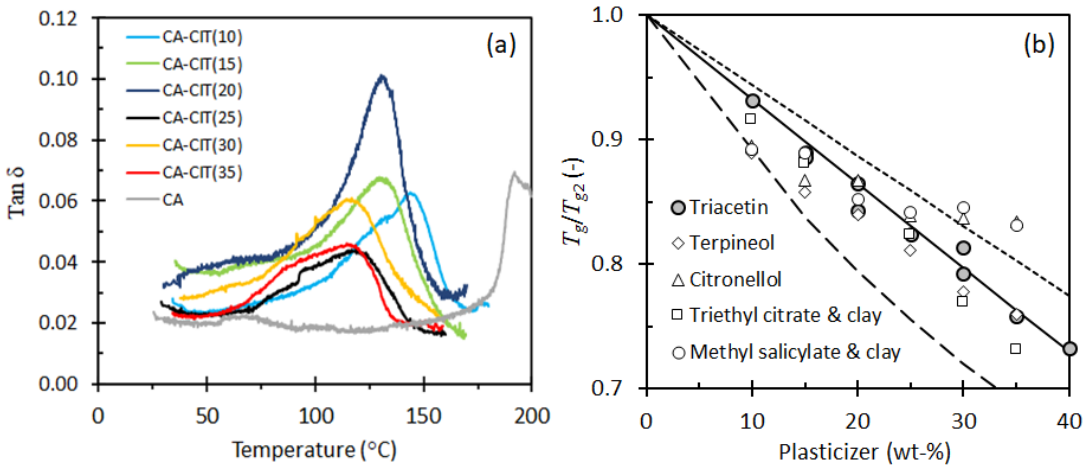

Fig. 4 (a) DMA curves showing tan delta peaks for cellulose diacetate films containing citronellol. (b) Experimental data showing the ratio of measured glass transition temperatures to that of the neat polymer. The solid circles are experimental values for triacetin and the solid line is the regressed linear dependence indicated by Mauritz et al. (1990). The dotted line represents the linear blending rule and the broken line the predictions of the Fox (1956) as applied to triacetin as a plasticizer

Amount of AC in the matrices

Details of the strands prepared by extrusion-compounding are provided in Table 2. The active content in the cellulose diacetate strands was determined by solvent extraction and thermogravimetric analysis. Both methods indicated values that were a little lower than the nominal amounts based on the quantities weighed out prior to extrusion-compounding. The discrepancy was, in some cases as high as 5 wt-%. This means that some of the active compounds were lost, probably attributable to vaporization due to their high volatility, during the extrusion-compounding process.

Table 3 Amount of active compound contained by the extruded strands

	Active compound content (wt-%)		
Active compound	**Nominal**	**TGA**	**Solvent extraction**
Citronellol	25	24.0	23.4 ± 0.2
	35	35.5	35.0 ± 0.2
Terpineol	25	20.7	23.1 ± 0.5
	35	32.2	33.4 ± 0.6
Methyl salicylate	25	21.7	23.4 ± 0.3
	35	33.8	34.2 ± 0.2

Scanning electron microscopy (SEM)

Fig. 5 shows the internal morphology of the strands, which initially contained 35 wt-% of the active compounds, after solvent extraction. The images show that the type of active compound affects the internal morphology of the

strand. Without the clay, the morphology of citronellol (Fig. 5a) and terpineol (Fig. 5c) strands exhibits characteristics of a homogenous system. The methyl salicylate strand (Fig. 5e) had a porous structure, due to the reduced compatibility and mixing efficiency at this concentration (35 wt-%), likely a result of exceeding the CA-methyl salicylate solubility limit. Most importantly, the incorporation of the organoclay significantly changed the morphology of the strands in all formulations. CA-clay strands containing Citronellol (Fig. 5b), terpineol (Fig. 5d) and methyl salicylate (Fig. 5f) all displayed a rough surface morphology consisting of irregular pore structures, which were most likely formed due to the clay dispersion and intercalation, confirmed by TEM images in Fig. 6.

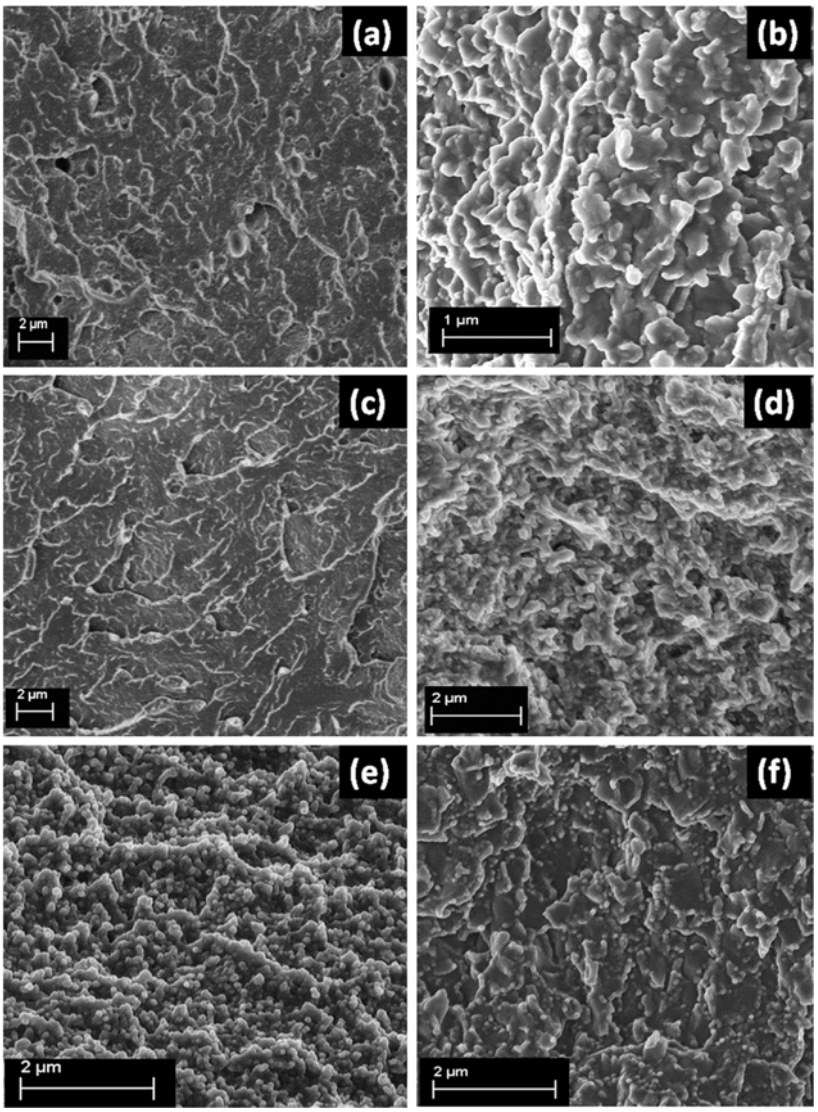

Fig. 5 SEM images showing the internal morphology of extruded CA strands that initially contained 35 wt-% of the active compounds, after solvent extraction. (a) Citronellol, (b) citronellol + 5 wt-% clay, (c) terpineol, (d) terpineol + 5 wt-% clay, (e) methyl salicylate, (f) methyl salicylate + 5 wt-% clay

Transmission electron microscopy (TEM)

The clay nanocomposite strands exhibited a combination of intercalation and tactoid formation of the clay nanoplatelets as presented in Fig. 6, which is consistent with previously studies (Rodríguez et al., 2019, Kaneko et al., 2013), which was also attributed to the high active compound content in the formulations, which also explains the absence of clay exfoliation in the matrices (Park et al., 2004). Furthermore, the clay nanoplatelets were well dispersed and almost randomly oriented, especially the citronellol and methyl salicylate strands, whereas the terpineol strand showed a more consistent orientation of the clay nanoplatelets in the matrix.

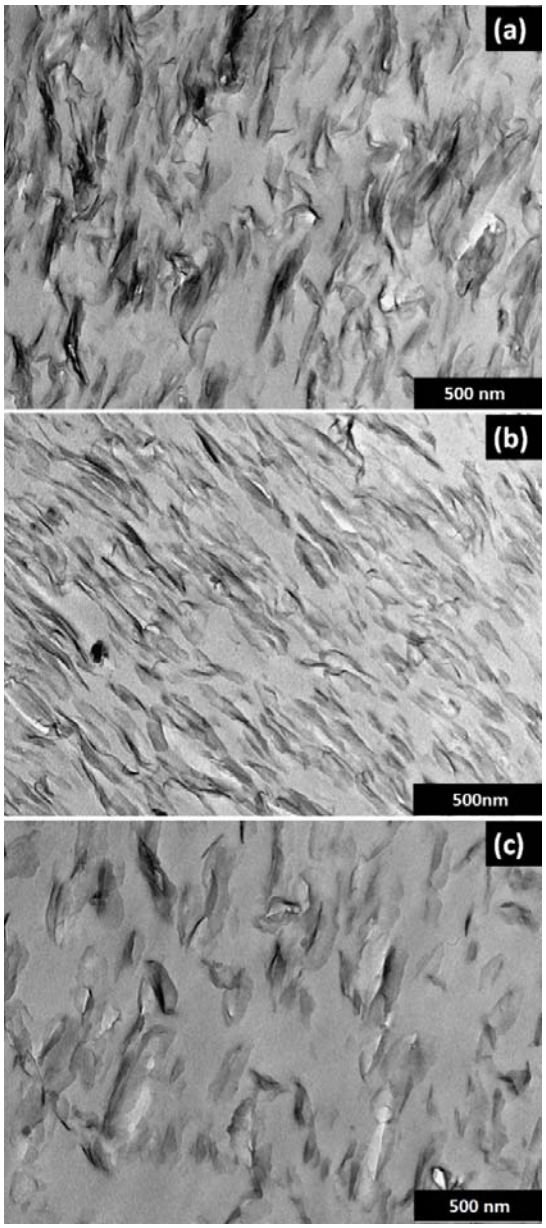

Fig. 6 TEM images of CA-clay nanocomposite strands that initially contained 35 wt-% (a) citronellol, (b) terpineol, and (c) methyl salicylate, after solvent extraction

Release profiles of active compounds from extruded strands

Release profiles of active compounds from the cellulose diacetate/organoclay matrix were determined by ageing the extruded strands for a period of 70 days in a convection oven set at 40 °C. Thereafter, least squares data regression was applied using the following models: Higuchi (Equation 8), log-logistic (Equation 10), Weibull (Equation 11), Modified Weibull (Equation 12) and diffusion (Equation 15). Direct regression resulted in values for β in the Weibull and the log-logistic models that were close to one-half. Therefore, the regressions with these two models were repeated enforcing $\beta = 0.5$ in Equation 10 and in Equation 11. Finally, for Equations 12 and 15, the relationship indicated by Equation 13 was enforced. This means that, in all models, only one single parameter, i.e. a characteristic time constant was allowed to vary freely. The correlation coefficient was used to rank the performance of the different models. Details of the regression results are presented in Table 4.

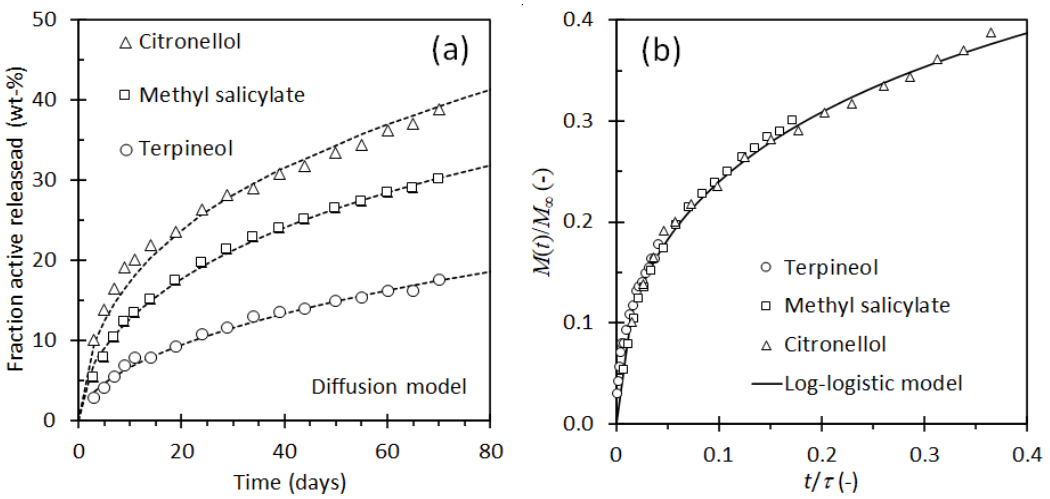

Fig. 7 (a) Release profiles of the active compounds obtained at 40 °C from cellulose diacetate strands which contained nominally 35 wt-% active compound. The broken lines show least squares regression based on the diffusion model, Equation 15. (b) Plot of normalized release curves against time normalized with respect to the characteristic time constant τ determined by least squares data regression

Fig. 7 shows that both the diffusion and log-logistic models gave good fits to the release data obtained for the cellulose diacetate/clay strands containing 35 wt-% of each active compound. The observed curvature of the experimental data is consistent with diffusion-limited release of the active compounds. Citronellol was released the fastest, followed by methyl salicylate and terpineol. This ranking differs from the volatility rankings based on vapor pressure and air permeability found previously, which is not surprising as the assumption is that the rate limiting step is diffusion inside the polymer matrix. This is then followed by evaporation of the compounds from the surface of the strands. All three active compounds feature an alcohol group in their structure that would be able to form intermolecular hydrogen bonds with the polymer matrix, which also affects their release rate from the matrix. The difference in the release rates was due to the significant differences in the compatibility of the active compounds with cellulose diacetate. Citronellol had the least compatibility for cellulose diacetate, verified by solubility parameters (Table 2), and least plasticization efficiency, confirmed by DMA (Fig. 4). Therefore, it

would diffuse from the matrix much faster due to relatively weaker C=O and -OH hydrogen bonds (from FTIR), compared to methyl salicylate and terpineol. Moreover, the release profiles were significantly improved by the incorporation of the clay in the matrices.

Table 4 Release models and their respective parameters for cellulose diacetate/organoclay nanocomposite strands containing active compounds at 25 and 35 wt-%

	Active	**Citronellol**		**Methyl salicylate**		**Terpineol**	
Model	**wt-%**	**25**	**35**	**25**	**35**	**25**	**35**
Higuchi	τ (days)	690	413	5074	708	23141	2233
	R	0.983	0.993	0.992	0.994	0.960	0.995
Diffusion	τ_o (days)	580	316	5181	617	25089	2183
$n = -4$	τ_1 (days)	511	279	4562	543	22094	1922
	R	0.986	0.996	0.995	0.998	0.981	0.996
Log-logistic	τ_o (days)	381	192	4335	407	23143	1677
$\beta = 0.5$	R	0.992	0.998	0.992	0.997	0.965	0.997
Weibull	τ (days)	507	279	4748	536	24098	1933
$\beta = 0.5$	R	0.986	0.996	0.993	0.997	0.966	0.996
Weibull-M	τ_1 (days)	561	330	5175	588	24151	1981
	τ_2 (days)	494	291	4562	518	21268	1744
	R	0.982	0.992	0.996	0.996	0.981	0.996

R – correlation coefficient.

Effect of strand diameter on release profiles

Equation 3 implies, and Equation 13 embodies, the notion that the release rate is characterised by a single characteristic time constant τ_o, i.e. $M(t)/M_\infty = g\left(t/\tau_o\right)$. Furthermore, τ_o is proportional to the square of the strand diameter and inversely proportional to the diffusion coefficient, i.e. $\tau \propto d^2/D$. Therefore, the expectation is that the release curves for strands with a diameter of d can be predicted by scaling the characteristic time constant τ_o, obtained experimentally for a strand with diameter d_o, by $\tau = \left(d/d_o\right)^2 \tau_o$. The diameters of the strands are presented in Table 5, and Figure 9 shows predictions based on the log-logistic model for strands containing 35 wt-% citronellol. Furthermore, the strand diameter was both halved and doubled to indicate its effect on the release curves. The predictions show that citronellol would be released more rapidly from the smaller diameter strand due to the higher surface area per unit volume. Therefore, the strand diameter will require careful attention when preparing these materials, and to ensure an optimal release of the active compound.

Table 5 Diameters of the extruded CA-clay strands containing active compounds at 25 and 35 wt-%

Nominal wt-%	Strands containing active compounds		
	Citronellol	Terpineol	Methyl salicylate
25	4.1 ± 0.8	4.8 ± 0.4	4.9 ± 0.7
35	3.5 ± 0.6	5.2 ± 1.3	5.4 ± 0.9

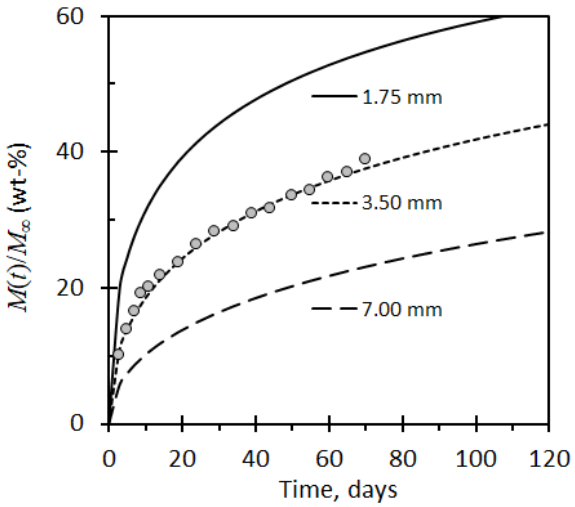

Fig. 8 The effect of strand diameter on the release curves expected for strands containing 35 wt-% citronellol. The predicted curves are based on the log-logistic equation

Conclusions

Biodegradable cellulose diacetate/organoclay nanocomposites containing plant-based insect attractants and repellents (at 25 and 35 wt-% active compound) were successfully prepared by extrusion-compounding. TGA verified the stability of the organoclay, cellulose diacetate and the selected active compounds at processing temperatures, i.e., 170 °C, a maximum temperature that was used to compound the polymer-organoclay nanocomposites with the selected active compounds. The processing temperature was sufficiently high to facilitate the CA & AC mixing, and yet low enough to avoid excessive AC loss and degradation of polymer. Furthermore, solvent extraction and TGA results showed that less than 5 wt-% was of the active compounds was lost by evaporation during the compounding process. DMA results proved that citronellol, terpineol and methyl salicylate can indeed function as plasticizers for cellulose diacetate. Therefore, the strands were prepared without the incorporation of conventional plasticizers. SEM images of the strands showed that the type of active compound and incorporation of the organoclay significantly modified the internal morphology of the strands. Moreover, TEM provided evidence of clay dispersion and intercalation, which also improved the release profiles of the active compounds. Oven ageing of the extruded strands at 40 °C showed that the active compounds were released form the nanocomposite matrix at a slow and controlled rate for a sufficiently long period, which suggests the possibility of developing long-life pest control devices.

Acknowledgements

Financial support from the Paper Manufacturers Association of South Africa (PAMSA) and the Department of Science and Innovation (DSI) under Grant DST/CON 0004/2019, and the National Research Foundation of South Africa (NRF) (Grant No. 130591) is gratefully acknowledged. The authors also express their gratitude to Laviosa Chimica Mineraria S.p.A (Italy) for providing the Dellite 43B organoclay sample, and Mr Farirai Ashly Matshaba for his assistance with compounding experiments.

Author Contributions

T.N.M: Conceptualization, planning, experimental work, data analysis, drafting of original manuscript and editing. **A.B.M:** Assistance with experimental work, data analysis, editing and validation. **J. W-S:** Electron microscopy, editing of manuscript and validation. **S.R:** Editing and validation. **W.W.F:** Conceptualization, planning, data analysis, editing of manuscript, validation, supervision, and funding acquisition. All authors read and approved the final version of the manuscript.

Declarations

The authors declare no competing interests.

Ethics approval

No results of studies involving humans or animals are reported.

References

ALLSOPP, E., PRINSLOO, G.J., SMART, L.E., DEWHIRST, S.Y. 2014. Methyl salicylate, thymol and carvacrol as oviposition deterrents for Frankliniella occidentalis (Pergande) on plum blossoms. *Anthropod-Plant Interactions,* 8**,** 421-427.

BAO, C. 2015. *Cellulose acetate/plasticizer systems:structure, morphology and dynamics.* PhD, Université Claude Bernard - Lyon.

BAO, C. Y., LONG, D. R. & VERGELATI, C. 2015. Miscibility and dynamical properties of cellulose acetate/plasticizer systems. *Carbohydr Polym,* 116**,** 95-102.

BATISTA, M., GUIRARDELLO, R. & KRAEHENBUEHL, M. 2015. Determination of the Hansen Solubility Parameters of Vegetable Oils, Biodiesel, Diesel, and Biodiesel-Diesel Blends. *Journal of the American Oil Chemists' Society,* 92**,** 95-109.

BIER, J. M., VERBEEK, C. J. R. & LAY, M. C. 2012. Identifying transition temperatures in bloodmeal-based thermoplastics using material pocket DMTA. *Journal of Thermal Analysis and Calorimetry,* 112**,** 1303-1315.

BOTHA, C. E. J., SACRAINE, S., GALLAGHER, S. & HILL, J. M. 2017. Russian wheat aphids: Breakfast, lunch & supper. Feasting on small grains in South Africa. *South African Journal of Botany,* 109**,** 154-173.

BRIGHAM, C. 2018. Chapter 3.22 - Biopolymers: Biodegradable Alternatives to Traditional Plastics. *In:* TÖRÖK, B. & DRANSFIELD, T. (eds.) *Green Chemistry.* Elsevier.

CHERMENSKAYA, T. D., BUROV, V. N., MANIAR, S. P., POW, E. M., RODITAKIS, N., SELYSKAYA, O. G., SHAMSHEV, I. V., WADHMAS, L. J. & WOODCOCK, C. M. 2001. Behavioural responses of

western flower thrips Frankliniella occidentalis (Pergande) to volatiles from three aromatic plants. *Insect Sci. Appl.,* 21**,** 67-72.
CHURCHILL, S. W. 2001. Correlating Equations for Transitional Behavior. *Industrial & Engineering Chemistry Research,* 40**,** 3053-3057.
CHURCHILL, S. W. & USAGI, R. 1972. A general expression for the correlation of rates of transfer and other phenomena. *AIChE Journal,* 18**,** 1121-1128.
COOK, S. M., KHAN, Z. R. & PICKETT, J. A. 2007. The use of push-pull strategies in integrated pest management. *Annual Review of Entomology.*
CRANK, J. 1975. *The Mathematics of Diffusion,* Oxford, Clarendon Press.
DARDOURI, T., GOMEZ, L., SCHOENY, A., COSTAGLIOLA, G. & GAUTIER, H. 2019. Behavioural response of green peach aphid Myzus persicae (Sulzer) to volatiles from different rosemary (Rosmarinus officinalis L.) clones. *Agricultural and Forest Entomology,* 21**,** 336-345.
DE PAULA, A. C., ULIANA, F., DA SILVA FILHO, E. A., SOARES, K. & LUZ, P. P. 2019. Use of DMA-material pocket to determine the glass transition temperature of nitrocellulose blends in film form. *Carbohydr Polym,* 226**,** 115288.
DREUX, X., MAJESTE, J. C., CARROT, C., ARGOUD, A. & VERGELATI, C. 2019. Viscoelastic behaviour of cellulose acetate/triacetin blends by rheology in the melt state. *Carbohydr Polym,* 222**,** 114973.
ERDMANN, R., KABASCI, S. & HEIM, H. P. 2021. Thermal Properties of Plasticized Cellulose Acetate and Its beta-Relaxation Phenomenon. *Polymers (Basel),* 13.
EWALD, J. A., WHEATLEY, C. J., AEBISCHER, N. J., MOREBY, S. J., DUFFIELD, S. J., CRICK, H. Q. P. & MORECROFT, M. B. 2015. Influences of extreme weather, climate and pesticide use on invertebrates in cereal fields over 42 years. *Global Change Biology,* 21**,** 3931-3950.
FEI, P., LIAO, L., CHENG, B. & SONG, J. 2017. Quantitative analysis of cellulose acetate with a high degree of substitution by FTIR and its application. *Analytical Methods,* 9**,** 6194-6201.
FERFERA-HARRAR, H. & DAIRI, N. 2014. Green nanocomposite films based on cellulose acetate and biopolymer-modified nanoclays: studies on morphology and properties. *Iranian Polymer Journal,* 23**,** 917-931.
FOX, T. G. 1956. Influence of Diluent and of Copolymer Composition on the Glass Temperature of a Polymer System. *Bull. Am. Phys. Soc.,* 1**,** 123.
GARCIA, M. T., GRACIA, I., DUQUE, G., LUCAS, A. & RODRIGUEZ, J. F. 2009. Study of the solubility and stability of polystyrene wastes in a dissolution recycling process. *Waste Manag,* 29**,** 1814-8.
GHORANI, B., RUSSELL, S. J. & GOSWAMI, P. 2013. Controlled Morphology and Mechanical Characterisation of Electrospun Cellulose Acetate Fibre Webs. *International Journal of Polymer Science,* 2013**,** 1-12.
GOPI, S., PIUS, A., KARGL, R., KLEINSCHEK, K. S. & THOMAS, S. 2019. Fabrication of cellulose acetate/chitosan blend films as efficient adsorbent for anionic water pollutants. *Polymer Bulletin,* 76**,** 1557-1571.
GUERRIERI, E. & DIGILIO, M. C. 2008. Aphid-plant interactions: a review. *Journal of Plant Interactions,* 3**,** 223-232.
HARDIE, J., ISAACS, R., PICKETT, J. A., WADHAMS, L. J. & WOODCOCK, C. M. 1994. Methyl salicylate and (-)-(1 R,5 S)-myrtenal are plant-derived repellents for black bean aphid, Aphis fabae Scop. (Homoptera: Aphididae). *Journal of Chemical Ecology,* 20**,** 2847-2855.
HIGUCHI, T. 1961. Rate of release of medicaments from ointment bases containing drugs in suspension. *J Pharm Sci,* 50**,** 874-5.
IGNACIO, M., CHUBYNSKY, M. V. & SLATER, G. W. 2017. Interpreting the Weibull fitting parameters for diffusion-controlled release data. *Physica A: Statistical Mechanics and its Applications,* 486**,** 486-496.
JATOI, A. W., OGASAWARA, H., KIM, I. S. & NI, Q. Q. 2020. Cellulose acetate/multi-wall carbon nanotube/Ag nanofiber composite for antibacterial applications. *Mater Sci Eng C Mater Biol Appl,* 110**,** 110679.
KANEKO, M. L. Q. A., ROMERO, R. B., DE PAIVA, R. E. F., FELISBERTI, M. I., GONÇALVES, M. C. & YOSHIDA, I. V. P. 2013. Improvement of toughness in polypropylene nanocomposite with the addition of organoclay/silicone copolymer masterbatch. *Polymer Composites,* 34**,** 194-203.
KOSCHIER, E. H. 2008. Essential Oil Compounds for Thrips Control – a Review. *Natural Product Communications,* 3**,** 1934578X0800300726.
KOSCHIER, E. H., DE KOGEL, W. J. & VISSER, J. H. 2000. Assessing the attractiveness of volatile plant compounds to western flower thrips *Frankliniella occidentalis*. *Journal of Chemical Ecology,* 26**,** 2643-2655.
KOSINA, J., DEWULF, J., VIDEN, I., POKORSKA, O. & VAN LANGENHOVE, H. 2013. Dynamic capillary diffusion system for monoterpene and sesquiterpene calibration: quantitative measurement and

determination of physical properties. *International Journal of Environmental Analytical Chemistry,* 93**,** 637-649.
KOSMIDIS, K., ARGYRAKIS, P. & MACHERAS, P. 2003. A Reappraisal of Drug Release Laws Using Monte Carlo Simulations: The Prevalence of the Weibull Function. *Pharmaceutical Research,* 20**,** 988-995.
KOUL, O., WALIA, S. & DHALIWAL, G. S. 2008. Essential Oils as Green Pesticides Potential and Constraints. *Biopestic. Int.,* 4**,** 63-84.
KUJUR, A., YADAV, A., KUMAR, A., SINGH, P. P. & PRAKASH, B. 2019. Nanoencapsulated methyl salicylate as a biorational alternative of synthetic antifungal and aflatoxin B1 suppressive agents. *Environ Sci Pollut Res Int,* 26**,** 18440-18450.
LAW, J. H. & REGNIER, F. E. 1971. Pheromones. *Annual Review of Biochemistry,* 40**,** 533-548.
LEE, M., DEY, K. P. & LEE, Y. S. 2020. Complexation of methyl salicylate with beta-cyclodextrin and its release characteristics for active food packaging. *Food Sci Biotechnol,* 29**,** 917-925.
LEITE, L. S. F., BATTIROLA, L. C., DA SILVA, L. C. E. & GONÇALVES, M. D. C. 2016. Morphological investigation of cellulose acetate/cellulose nanocrystal composites obtained by melt extrusion. *Journal of Applied Polymer Science,* 133.
LOUWERSE, M. J., MALDONADO, A., ROUSSEAU, S., MOREAU-MASSELON, C., ROUX, B. & ROTHENBERG, G. 2017. Revisiting Hansen Solubility Parameters by Including Thermodynamics. *Chemphyschem,* 18**,** 2999-3006.
MAPOSSA, A. B., SITOE, A., FOCKE, W. W., IZADI, H., DU TOIT, E. L., ANDROSCH, R., SUNGKAPREECHA, C. & VAN DER MERWE, E. M. 2020. Mosquito repellent thermal stability, permeability and air volatility. *Pest Management Science,* 76**,** 1112-1120.
MARABI, A., LIVINGS, S., JACOBSON, M. & SAGUY, I. S. 2003. Normalized Weibull distribution for modeling rehydration of food particulates. *European Food Research and Technology,* 217**,** 311-318.
MARTIN, T., SAIDI, M., NIASSY, S., SIMON, S., VIDOGBENA, F., PARROT, L., EKESI, S., DELETRE, E., SUBRAMANIAN, S., ASSOGBA-KOMLAN, F., BAIRD, V., FIABOE, K. K. M., NGOUAJIO, M., SIMON, J. E. & RATNADASS, A. 2018. Insect net: a novel technology to promote integrated pest management on horticultural crops in Africa. *Acta Horticulturae***,** 43-52.
MAURITZ, K. A., STOREY, R. F. & WILSON, B. S. 1990. Efficiency of plasticization of PVC by higher-order di-alkyl phthalates and survey of mathematical models for prediction of polymer/diluent blend Tg's. *Journal of Vinyl Technology,* 12**,** 165-173.
MCBRIERTY, V. J., KEELY, C. M., COYLE, F. M., XU, H. & VIJ, J. K. 1996. Hydration and plasticization effects in cellulose acetate: molecular motion and relaxation. *Faraday Discussions,* 103**,** 255-268.
MILLER, J. R. & COWLES, R. S. 1990. Stimulo-deterrent diversion: A concept and its possible application to onion maggot control. *Journal of Chemical Ecology,* 16**,** 3197-3212.
OKHOVAT, A., ASHTIANI, F. Z. & KARIMI, M. 2015. A comparative study on thermodynamic phase behavior analysis of cellulose acetate, cellulose acetate propionate and cellulose acetate butyrate-DMF-water ternary systems. *Journal of Polymer Research,* 22**,** 234.
PAPADOPOULOU, V., KOSMIDIS, K., VLACHOU, M. & MACHERAS, P. 2006. On the use of the Weibull function for the discernment of drug release mechanisms. *International Journal of Pharmaceutics,* 309**,** 44-50.
PARK, H. M., MISRA, M., DRZAL, L. T. & MOHANTY, A. K. 2004. "Green" nanocomposites from cellulose acetate bioplastic and clay: effect of eco-friendly triethyl citrate plasticizer. *Biomacromolecules,* 5**,** 2281-8.
PHUONG, V. T., VERSTICHE, S., CINELLI, P., ANGUILLESI, I., COLTELLI, M.-B. & LAZZERI, A. 2014. Cellulose Acetate Blends - Effect of Plasticizers on Properties and Biodegradability. *Journal of Renewable Materials,* 2**,** 35-41.
PICARD, I., HOLLINGSWORTH, R. G., SALMIERI, S. & LACROIX, M. 2012. Repellency of essential oils to Frankliniella occidentalis (Thysanoptera: Thripidae) as affected by type of oil and polymer release. *J Econ Entomol,* 105**,** 1238-47.
PIETERSE, N. & FOCKE, W. W. 2003. Diffusion-controlled evaporation through a stagnant gas: estimating low vapour pressures from thermogravimetric data. *Thermochimica Acta,* 406**,** 191-198.
POTTS, S. G., BIESMEIJER, J. C., KREMEN, C., NEUMANN, P., SCHWEIGER, O. & KUNIN, W. E. 2010. Global pollinator declines: Trends, impacts and drivers. *Trends in Ecology and Evolution,* 25**,** 345-353.
PULS, J., WILSON, S. A. & HÖLTER, D. 2010. Degradation of Cellulose Acetate-Based Materials: A Review. *Journal of Polymers and the Environment,* 19**,** 152-165.
QUINTANA, R., PERSENAIRE, O., LEMMOUCHI, Y., SAMPSON, J., MARTIN, S., BONNAUD, L. & DUBOIS, P. 2013. Enhancement of cellulose acetate degradation under accelerated weathering by plasticization with eco-friendly plasticizers. *Polymer Degradation and Stability,* 98**,** 1556-1562.

RITGER, P. L. & PEPPAS, N. A. 1987. A simple equation for description of solute release I. Fickian and non-fickian release from non-swellable devices in the form of slabs, spheres, cylinders or discs. *Journal of Controlled Release,* 5**,** 23-36.

RODRÍGUEZ, F. J., ABARCA, R. L., BRUNA, J. E., MOYA, P. E., GALOTTO, M. J., GUARDA, A. & PADULA, M. 2019. Effect of organoclay and preparation method on properties of antimicrobial cellulose acetate films. *Polymer Composites,* 40**,** 2311-2319.

SAID-AL AHL, H. A. H., HIKAL, W. M. & TKACHENKO, K. G. 2017. Essential Oils with Potential as Insecticidal Agents: A Review. *International Journal of Environmental Planning and Management,* 3**,** 23-33.

SIEPMANN, J. & PEPPAS, N. A. 2011. Higuchi equation: Derivation, applications, use and misuse. *International Journal of Pharmaceutics,* 418**,** 6-12.

SILVA, T. N. D., REYNAUD, F., PICCIANI, P. H. S., DE HOLANDA, E. S. K. G. & BARRADAS, T. N. 2020. Chitosan-based films containing nanoemulsions of methyl salicylate: Formulation development, physical-chemical and in vitro drug release characterization. *Int J Biol Macromol,* 164**,** 2558-2568.

SONGKRO, S., HAYOOK, N., JAISAWANG, J., MANEENUAN, D., CHUCHOME, T. & KAEWNOPPARAT, N. 2011. Investigation of inclusion complexes of citronella oil, citronellal and citronellol with β-cyclodextrin for mosquito repellent. *Journal of Inclusion Phenomena and Macrocyclic Chemistry,* 72**,** 339-355.

SUDIARTI, T., WAHYUNINGRUM, D., BUNDJALI, B. & ARCANA, I. M. 2017. Mechanical strength and ionic conductivity of polymer electrolyte membranes prepared from cellulose acetate-lithium perchlorate. *IOP Conference Series: Materials Science and Engineering,* 223**,** 012052.

SWAPNIL, S. I., DATTA, N., MAHMUD, M. M., JAHAN, R. A. & ARAFAT, M. T. 2020. Morphology, mechanical, and physical properties of wet-spun cellulose acetate fiber in different solvent-coagulant systems and in-situ crosslinked environment. *Journal of Applied Polymer Science,* 138**,** 50358.

TEIXEIRA, S. C., SILVA, R. R. A., DE OLIVEIRA, T. V., STRINGHETA, P. C., PINTO, M. R. M. R. & SOARES, N. D. F. F. 2021. Glycerol and triethyl citrate plasticizer effects on molecular, thermal, mechanical, and barrier properties of cellulose acetate films. *Food Bioscience,* 42**,** 101202.

TERAMOTO, Y. 2015. Functional thermoplastic materials from derivatives of cellulose and related structural polysaccharides. *Molecules,* 20**,** 5487-527.

WYPYCH, G. 2019. 4.1.4 Hansen's Solubility. *In: Handbook of Solvents, Volume 1 - Properties (3rd Edition).* ChemTec Publishing.

YOU, C., GUO, S., ZHANG, W., YANG, K., GENG, Z., DU, S., WANG, C. & DENG, Z. 2015. Identification of Repellent and Insecticidal Constituents fromArtemisia mongolicaEssential Oil againstLasioderma serricorne. *Journal of Chemistry,* 2015**,** 1-7.

ZEPNIK, S., HILDEBRAND, T., KABASCI, S., RA-DUSCH, H.-J. & WODKE, T. 2013a. Cellulose Acetate for Thermoplastic Foam Extrusion.

ZEPNIK, S., KABASCI, S., KOPITZKY, R., RADUSCH, H.-J. & WODKE, T. 2013b. Extensional Flow Properties of Externally Plasticized Cellulose Acetate: Influence of Plasticizer Content. *Polymers,* 5**,** 873-889.

ZHANG, Q., FANG, C., CHENG, Y., CHEN, J., HUANG, Z. & HAN, H. 2020. Construction and properties of cellulose diacetate film derived from waste cigarette filters. *Cellulose,* 27**,** 8899-8907.